Reduction–Oxidation Properties of Organotransition-metal Complexes. Part 30.[1] Triazenido-bridged Carbonylrhodium Bipyridyl Complexes with $[Rh_2]^{2+}$, $[Rh_2]^{3+}$, and $[Rh_2]^{4+}$ cores, and the *X*-Ray Structures of $[Rh_2(CO)_2(bipy)(\mu\text{-RNNNR})_2]\text{-}[BF_4]\cdot CH_2Cl_2$ and $[\{Rh_2I(CO)(bipy)(\mu\text{-RNNNR})_2\}_2][PF_6]_2\cdot 2.5CH_2Cl_2$ (R = *p*-tolyl)*

Thomas Brauns, Carmen Carriedo, John S. Cockayne, Neil G. Connelly, Gabriel Garcia Herbosa, and A. Guy Orpen
Department of Inorganic Chemistry, University of Bristol, Bristol BS8 1TS

The reaction of $[\{Rh(CO)_2(\mu\text{-RNNNR})\}_2]$ (**1**; R = *p*-tolyl) with 2,2′-bipyridyl (bipy) in boiling n-heptane gives $[Rh_2(CO)_2(bipy)(\mu\text{-RNNNR})_2]$ (**2**) which undergoes two one-electron oxidations at a platinum-bead electrode in CH_2Cl_2. Chemical oxidation of (**2**) with $[Fe(\eta\text{-}C_5H_5)_2]^+$ gives $[Rh_2(CO)_2(bipy)(\mu\text{-RNNNR})_2]^+$ ($\mathbf{2}^+$) the *X*-ray structure of which, as a dichloromethane solvate of the $[BF_4]^-$ salt, shows a Rh–Rh separation of 2.646(1) Å consistent with a formal metal–metal bond order of 0.5. The cation ($\mathbf{2}^+$) undergoes carbonyl substitution reactions with PPh_3 or $P(OPh)_3$ to give $[Rh_2(CO)L(bipy)(\mu\text{-RNNNR})_2][PF_6]$ ($\mathbf{3}^+$), and with iodide ion to yield $[Rh_2I(CO)(bipy)(\mu\text{-RNNNR})_2]$ (**4**) which may also be prepared directly from (**2**) and iodine at −78 °C. The cyclic voltammogram of (**4**) in CH_2Cl_2 shows one reduction and three oxidation waves; chemical oxidation of (**4**) with $[Fe(\eta\text{-}C_5H_5)_2][PF_6]$ gives the tetranuclear complex $[\{Rh_2I(CO)\text{-}(bipy)(\mu\text{-RNNNR})_2\}_2][PF_6]_2$ (**5**). *X*-Ray structural studies on the CH_2Cl_2 solvate of (**5**) show that the dication is centrosymmetric, having two binuclear ($\mathbf{4}^+$) units [Rh–Rh distance within each, 2.544(1) Å] linked by asymmetric iodide bridges, $Rh\text{–}I_{axial}$ 2.760(1) Å and $Rh\text{–}I_{equatorial}$ 2.670(1) Å. Complex (**5**) reacts with I^- to give $[Rh_2I_2(CO)(bipy)(\mu\text{-RNNNR})_2]$ (**6**), which may also be made directly from (**2**) and iodine, and with $Na[S_2CNMe_2]$ to yield $[Rh_2(CO)(S_2CNMe_2)(bipy)\text{-}(\mu\text{-RNNNR})_2][PF_6]$ (**7**). The complexes [$\mathbf{3}^+$; L = PPh_3 or $P(OPh)_3$] react with chloride ion in the presence of $[Fe(\eta\text{-}C_5H_5)_2][PF_6]$ giving $[Rh_2Cl(CO)L(bipy)(\mu\text{-RNNNR})_2][PF_6]$ [**8**; L = PPh_3 or $P(OPh)_3$]. Both (**7**) and (**8**) undergo one-electron oxidation and reduction at a platinum electrode. The mechanism of the oxidative addition of iodine to (**2**) to give (**5**), and the low-temperature e.s.r. spectra of the paramagnetic $[Rh_2]^{3+}$ complexes ($\mathbf{2}^+$), ($\mathbf{3}^+$), and (**4**), are discussed.

We have recently shown that $[\{Rh(CO)_2(\mu\text{-RNNNR})\}_2]$ (**1**), (throughout this paper R = *p*-tolyl), $[\{Rh(CO)_2[\mu\text{-PhNC}(Me)NPh]\}_2]$,[2] and $[\{Ir(CO)_2(\mu\text{-RNNNR})\}_2]$[3] and their Lewis base and η^4-diene derivatives are oxidised to paramagnetic, $[Rh_2]^{3+}$-containing delocalised mixed-valence complexes. In an attempt to produce trapped-valence analogues, perhaps capable of sustaining photochemically induced intramolecular electron-transfer reactions, we have investigated the synthesis of geometrically asymmetric derivatives of (**1**). We now give details[4] of the preparation of $[Rh_2(CO)_2(bipy)(\mu\text{-RNNNR})_2]$ (**2**) (bipy = 2,2′-bipyridyl) (Scheme 1) the precursor to a range of redox-active, $[Rh_2]^{3+}$- and $[Rh_2]^{4+}$-containing species including $[Rh_2(CO)_2(bipy)(\mu\text{-RNNNR})_2][BF_4]$ and $[\{Rh_2I\text{-}(CO)(bipy)(\mu\text{-RNNNR})_2\}_2][PF_6]_2$ which have been characterised by *X*-ray structural methods. We also comment on the mechanism of the oxidative addition of iodine to (**2**), and the low-temperature e.s.r. spectra of the new mixed-valence $[Rh_2]^{3+}$ complexes.

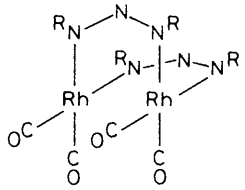

(**1**)

Results and Discussion

The reaction of $[\{Rh(CO)_2(\mu\text{-RNNNR})\}_2]$ (**1**) with bipy in n-heptane, under gentle reflux and with the rigorous exclusion of air, gave a high yield of $[Rh_2(CO)_2(bipy)(\mu\text{-RNNNR})_2]$ (**2**; Scheme 1) as air-sensitive black crystals (Table 1). The structure proposed for (**2**) [Figure 1(*a*)] differs from those adopted[2] by $[Rh_2(CO)_2(PPh_3)_2(\mu\text{-RNNNR})_2]$ [Figure 1(*b*)] and proposed for $[Rh_2(CO)_2(\mu\text{-}Ph_2PCH_2PPh_2)(\mu\text{-RNNNR})_2]$ [Figure 1(*c*)] in containing a *cis*-$Rh(CO)_2$ group, as shown by the presence of two i.r. carbonyl bands separated by 65 cm^{-1}. The ^1H n.m.r. spectrum, in C_6D_6, is also in agreement with the proposed structure, with two methyl resonances (δ 2.10 and 2.04) and four doublets (δ 8.45, 8.31, 7.06, and 6.98; *J* 8.1 Hz) for the inequivalent pairs of *p*-tolyl groups of the triazenide bridges, and four signals for the chelating bipy ligand (δ 8.59, d, 5.6 Hz; 6.85, t, 8.6 Hz; 6.72, d, 8.0 Hz, and 6.17, t, 6.2 Hz).

* 1-(2,2′-Bipyridyl)-2,2-dicarbonylbis(μ-di-*p*-tolyltriazenido-N^1N^3)-dirhodium tetrafluoroborate–dichloromethane (1/1) and, 1,4-bis[2,2′-bipyridyl-2,3-dicarbonyl-1,2;1,2;3,4;3,4-tetrakis(μ-di-*p*-tolyltriazenido-N^1N^3)]-2,3;2,3-di-μ-iodo-tetrarhodium(*Rh*^{1}–*Rh*^{2}, *Rh*^{3}–*Rh*^{4}) bis(hexafluorophosphate)–dichloromethane (2/5).

Supplementary data available: see Instructions for Authors, *J. Chem. Soc., Dalton Trans.*, 1989, Issue 1, pp. xvii—xx.

Non-S.I. unit employed: G = 10^{-4} T.

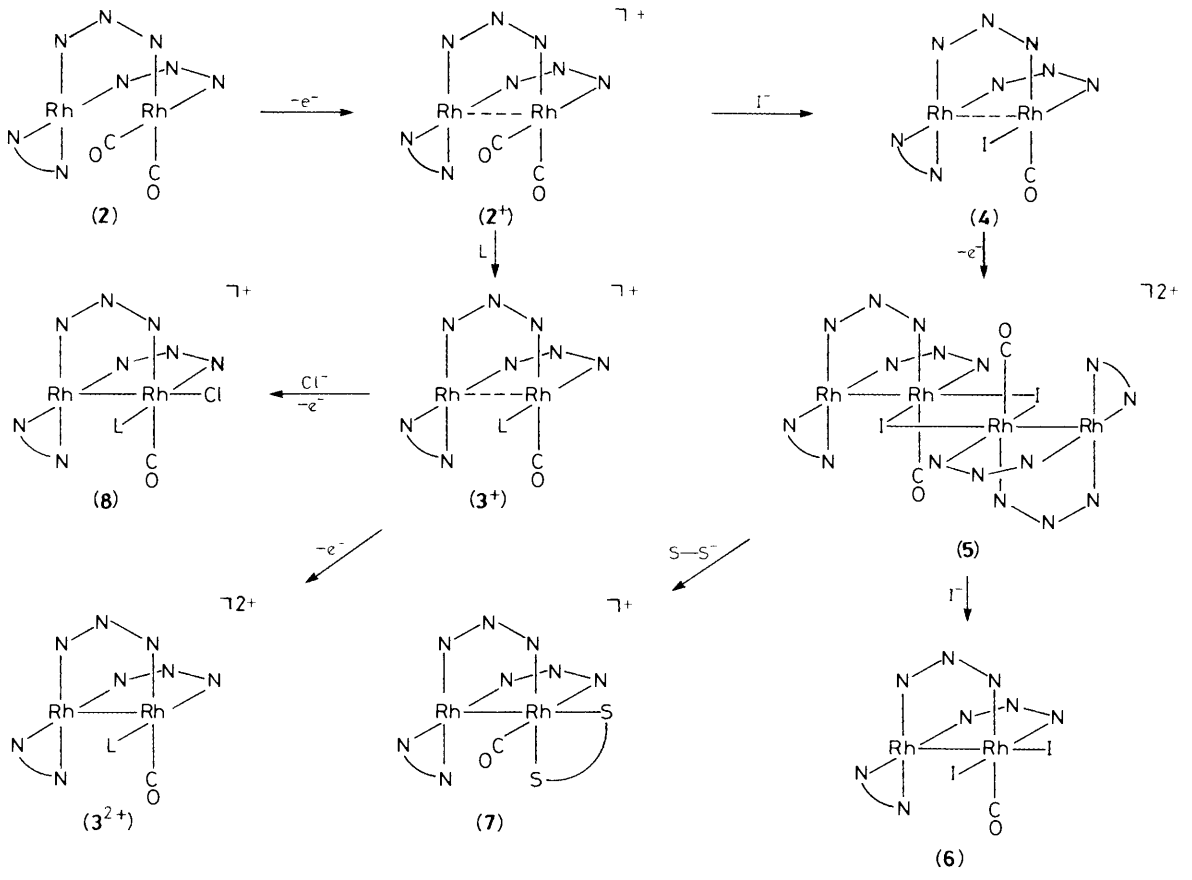

Scheme 1. NNN = *p*-$MeC_6H_4NNNC_6H_4Me$-*p*, N–N = 2,2′-bipyridyl, S–S = S_2CNMe_2, L = PPh_3 or $P(OPh)_3$

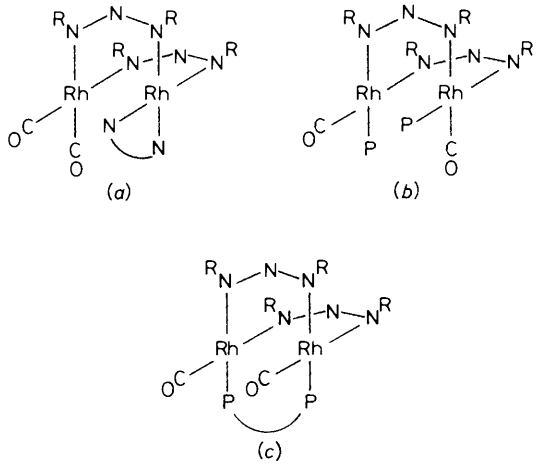

Figure 1. Structures of (*a*) $[Rh_2(CO)_2(bipy)(\mu\text{-}RNNNR)_2]$ (**2**), (*b*) $[Rh_2(CO)_2(PPh_3)_2(\mu\text{-}RNNNR)_2]$, and (*c*) $[Rh_2(CO)_2(\mu\text{-}Ph_2PCH_2PPh_2)(\mu\text{-}RNNNR)_2]$; R = *p*-tolyl

The cyclic voltammogram (c.v.) of complex (**2**) in CH_2Cl_2 shows two oxidation waves in the potential range −1.5 to +1.5 V (Table 2). The first wave is diffusion controlled and fully reversible* and corresponds to the formation of the monocation (2^+); the second wave is ill defined and will not be discussed further. The potential for the first oxidation (E° = −0.25 V) is much more negative than that of $[Rh_2(CO)_2(PPh_3)_2(\mu\text{-}RNNNR)_2]$ (E° = 0.18 V),[2] perhaps accounting for the air-sensitivity of (**2**) and certainly suggesting that the chemical synthesis of (2^+) should require the use of only a mild oxidant. Accordingly, treatment of (**2**) with $[Fe(\eta\text{-}C_5H_5)_2]^+$ in CH_2Cl_2 rapidly gave excellent yields of the air-stable, black crystalline $[BF_4]^-$ or $[PF_6]^-$ salts of the cation $[Rh_2(CO)_2(bipy)(\mu\text{-}RNNNR)_2]^+$ (2^+).

The i.r. carbonyl spectrum of (2^+) (Table 1) is similar to that of (**2**) except that the two bands are shifted to higher wavenumber, as expected on oxidation. In addition, the c.v. of the monocation is identical to that of the neutral precursor save that the wave at −0.25 V corresponds to a reduction (as confirmed by voltammetry at a rotating platinum electrode). These results suggest that the structures of (**2**) and (2^+) are grossly similar {*cf.* those of $[Rh_2(CO)_2(PPh_3)_2(\mu\text{-}RNNNR)_2]^Z$ (Z = 0 or 1) where the major change is a shortening of the metal–metal bond length on oxidation; the overall face-to-face geometry is retained}.[5] Thus, the *X*-ray crystal structure of $[Rh_2(CO)_2(bipy)(\mu\text{-}RNNNR)_2][BF_4]\cdot CH_2Cl_2$ has been determined as representative of both (2^+) and (**2**).

The structure of the cation $[Rh_2(CO)_2(bipy)(\mu\text{-}RNNNR)_2]^+$ is illustrated in Figure 2, and selected bond lengths and angles are listed in Table 3. The crystal structure consists of isolated (2^+) and $[BF_4]^-$ ions and CH_2Cl_2 solvent molecules. The shortest intermolecular Rh · · · Rh distance is 8.67 Å indicating no tendency to dimerisation between (2^+) ions in the solid

* Unless otherwise stated, all of the redox processes reported are diffusion controlled ($i/v^{\frac{1}{2}}$ = constant for scan rates $50 \leqslant v \leqslant 500$ mV s^{-1}) and fully reversible (*e.g.* for an oxidation process, i_{red}/i_{ox} = 1 for all scan rates used).

Table 1. Analytical and i.r. spectroscopic data for dirhodium complexes

Complex[a]	Colour	Yield (%)	Analysis (%)[b] C	H	N	$\tilde{\nu}$(CO)[c]/cm^{-1}
$[Rh_2(CO)_2(bipy)(\mu\text{-}L')_2]$ (**2**)	Black	82	54.9 (55.4)	4.2 (4.2)	12.7 (12.9)	2 027, 1 962
$[Rh_2(CO)_2(bipy)(\mu\text{-}L')_2][PF_6]$ (**2**$^+$)	Brown	80	47.2 (47.5)	3.6 (3.6)	10.7 (11.1)	2 095, 2 050
$[Rh_2(CO)(PPh_3)(bipy)(\mu\text{-}L')_2][PF_6]$ (**3**$^+$; L = PPh_3)	Brown	89	54.4 (54.9)	4.2 (4.1)	8.8 (9.0)	2 018
$[Rh_2(CO)\{P(OPh)_3\}(bipy)(\mu\text{-}L')_2][PF_6]$ [**3**$^+$; L = $P(OPh)_3$]	Brown	40	51.6 (51.6)[d]	4.1 (3.9)	8.1 (8.4)	2 037
$[Rh_2I(CO)(bipy)(\mu\text{-}L')_2]$ (**4**)	Brown	70	48.8 (48.5)	3.9 (3.8)	11.2 (11.6)	1 996
$[\{Rh_2I(CO)(bipy)(\mu\text{-}L')_2\}_2][PF_6]_2$ (**5**)	Black	87	40.1 (40.2)[e]	3.2 (3.2)	9.3 (9.4)	2 073
$[Rh_2I_2(CO)(bipy)(\mu\text{-}L')_2]$ (**6**)	Brown	79	43.2 (42.9)	3.5 (3.3)	10.2 (10.3)	2 027
$[Rh_2(CO)(S_2CNMe_2)(bipy)(\mu\text{-}L')_2][PF_6]$ (**7**)	Grey-green	45	45.5 (45.7)	3.9 (3.8)	11.3 (11.4)	2 060
$[Rh_2Cl(CO)(PPh_3)(bipy)(\mu\text{-}L')_2][PF_6]$ (**8**; L = PPh_3)	Green	47	52.8 (53.4)	4.2 (4.0)	8.8 (8.8)	2 043
$[Rh_2Cl(CO)\{P(OPh)_3\}(bipy)(\mu\text{-}L')_2][PF_6]$ [**8**; L = $P(OPh)_3$]	Green	45	50.9 (51.5)	4.0 (3.9)	8.0 (8.4)	2 062

[a] L′ = *p*-$MeC_6H_4NNNC_6H_4Me$-*p*. [b] Calculated values in parentheses. [c] In CH_2Cl_2. [d] Analysed as a 0.5 CH_2Cl_2 solvate. [e] Analysed as a 1.0 CH_2Cl_2 solvate.

Table 2. Cyclic voltammetric data[a] for dirhodium complexes (L′ = RNNNR, R = *p*-tolyl)

Complex	Couple E^o[b]/V $[Rh_2]^{2+/3+}$	$[Rh_2]^{3+/4+}$	$[Rh_2]^{4+/5+}$
$[Rh_2(CO)_2(bipy)(\mu\text{-}L')_2]$ (**2**)	−0.25	0.9 (I)	
$[Rh_2(CO)_2(bipy)(\mu\text{-}L')_2]^+$ (**2**$^+$)	−0.25	0.9 (I)	
$[Rh_2(CO)(PPh_3)(bipy)(\mu\text{-}L')_2]^+$ (**3**$^+$; L = PPh_3)	−0.53	0.78	1.47
$[Rh_2(CO)\{P(OPh)_3\}(bipy)(\mu\text{-}L')_2]^+$ [**3**$^+$; L = $P(OPh)_3$]	−0.42	0.82	1.47
$[Rh_2I(CO)(bipy)(\mu\text{-}L')_2]$ (**4**)	−1.07	0.21[c]	1.25[d]
			1.37
$[\{Rh_2I(CO)(bipy)(\mu\text{-}L')_2\}_2]^{2+}$ (**5**)	−1.08	0.21[c]	1.24[d]
			1.39
$[Rh_2(CO)(S_2CNMe_2)(bipy)(\mu\text{-}L')_2]^+$ (**7**)		−0.84[e]	1.13
$[Rh_2Cl(CO)(PPh_3)(bipy)(\mu\text{-}L')_2]^+$ (**8**; L = PPh_3)		−0.56	1.25[f]
$[Rh_2Cl(CO)\{P(OPh)_3\}(bipy)(\mu\text{-}L')_2]^+$ [**8**; L = $P(OPh)_3$]		−0.45	1.34[f]

[a] All processes are diffusion-controlled and one-electron, obeying the criterion $i/v^{\frac{1}{2}}$ = constant for scan rates, v, in the range 50—500 mV s^{-1}. [b] E^o values are reported for reversible processes, calculated as the average of the cathodic and anodic peak potentials unless stated otherwise. Peak potentials, E_{pk}, are reported for irreversible (I) processes, at v = 200 mV s^{-1} unless stated otherwise. All potentials are *versus* the aqueous s.c.e., at a platinum bead in CH_2Cl_2 with 0.1 mol dm^{-3} $[NBu^n_4][PF_6]$ as supporting electrolyte. Under these conditions, the E^o values for the couples $[Fe(\eta\text{-}C_5H_5)_2]^+$ $[Fe(\eta\text{-}C_5H_5)_2]$ and $[Fe(\eta\text{-}C_5Me_5)_2]^+$–$[Fe(\eta\text{-}C_5Me_5)_2]$ are 0.47 and −0.07 V respectively. [c] Average of the cathodic and anodic peak potentials of the wave associated with the processes shown in Scheme 2 (see text). [d] Potentials for the oxidations of the tetranuclear dication (**5**) to the trication, $[Rh_4]^{9+}$, and tetracation, $[Rh_4]^{10+}$ respectively (see text). [e] Further ill defined waves are observed at 1.5 and 1.8 V (oxidations) and −1.3 and −1.6 V (reductions). [f] A further, irreversible oxidation wave is observed at *ca.* 1.7 V.

state. The cation (**2**$^+$) has two rhodium atoms at a separation of 2.646(1) Å, somewhat shorter than in the $[Rh_2]^{3+}$ core of $[Rh_2(CO)_2(PPh_3)_2(\mu\text{-}RNNNR)_2]^+$ [2.698(1) Å].[5] The ligands around each rhodium form a planar array, with Rh(1) carrying two *cis*-carbonyl ligands, and Rh(2) the chelating 2,2′-bipyridyl ligand. As in the previously studied dirhodium bis-μ-triazenido species, the μ-RNNNR ligands occupy *cis* sites on each rhodium and the $Rh_2(\mu\text{-}NNN)_2$ fragment shows approximate C_2 symmetry. The C_2 geometry adopted involves a twist about the Rh–Rh vector (away from a C_{2v} arrangement), reflected in N–Rh–Rh–N torsion angles of −16.4 and −18.3° within the $Rh_2(\mu\text{-}RNNNR)$ groups of (**2**$^+$). The ligand co-ordination planes at each rhodium are tilted at an angle of 22.3° to one another {*cf.* comparable angles of 40.8 and 31.3° for $[Rh_2(CO)_2(PPh_3)_2(\mu\text{-}RNNNR)_2]$ and its cation}.[5] This reduction in tilt may be associated with the reduced bulk of the substituents at Rh [(bipy)$(CO)_2$ *vs.* $(PPh_3)_2(CO)_2$] as well as being a consequence of the Rh···Rh bond order (here formally 0.5, *cf.* 0 for $[Rh_2]^{2+}$ and 1 for $[Rh_2]^{4+}$ species).

Complex (**2**$^+$) is unlike the monocations of the dicarbonyls shown in Figure 1(*b*) and (*c*) in containing a substitutionally labile $Rh(CO)_2$ group. Thus, the room-temperature reactions of (**2**$^+$) with PPh_3 or $P(OPh)_3$ in CH_2Cl_2 readily give the brown, crystalline salts $[Rh_2(CO)L(bipy)(\mu\text{-}RNNNR)_2][PF_6]$ [**3**$^+$; L = PPh_3 or $P(OPh)_3$] (Table 1). The c.v.s of these complexes each show three reversible waves, one reduction and two oxidations, as illustrated in Figure 3 for (**3**$^+$; L = PPh_3). The products of these redox reactions could not be isolated although in CH_2Cl_2 (**3**$^+$; L = PPh_3) reacts with $AgPF_6$ and with $[NBu^n_4][BH_4]$ to give solutions with i.r. carbonyl bands at 2 054 and 1 952 cm^{-1} respectively; the shifts from the value of 2 018 cm^{-1} for (**3**$^+$; L = PPh_3) may indicate the formation of the dication (**3**$^{2+}$; L = PPh_3) and neutral molecule (**3**; L = PPh_3).

Carbonyl substitution of (**2**$^+$) also occurs with iodide ion, the room-temperature reaction in CH_2Cl_2 affording the black, air-sensitive solid $[Rh_2I(CO)(bipy)(\mu\text{-}RNNNR)_2]$ (**4**). This neutral complex, better prepared directly from (**2**) and iodine at −78 °C, is isoelectronic with [**3**$^+$; L = PPh_3 or $P(OPh)_3$] but its c.v. (Figure 4) differs markedly from those of the latter complexes.

First, the c.v. of (**4**) shows one reduction wave and *three* oxidation waves the relative heights of which appear to be in the ratio 2:2:1:1 (as also shown by voltammetry at a rotating platinum electrode). Secondly, the first oxidation wave has a peak-to-peak separation $[\Delta = (E_p)_{ox} - (E_p)_{red}]$ far greater than that either of any of the other waves or of the oxidation

Table 3. Selected bond lengths (Å) and angles (°) for the complex $(2^+)BF_4 \cdot CH_2Cl_2$

Rh(1)–Rh(2)	2.646(1)	Rh(1)–C(1)	1.890(12)	C(35)–C(36)	1.416(15)	C(41)–C(42)	1.386(13)
Rh(1)–C(2)	1.870(13)	Rh(1)–N(1)	2.070(9)	C(41)–C(46)	1.378(19)	C(41)–N(6)	1.439(13)
Rh(1)–N(4)	2.070(9)	Rh(2)–N(3)	2.039(9)	C(42)–C(43)	1.419(16)	C(43)–C(44)	1.359(21)
Rh(2)–N(6)	2.030(10)	Rh(2)–N(91)	2.056(10)	C(44)–C(45)	1.374(15)	C(44)–C(47)	1.517(17)
Rh(2)–N(9c)	2.045(9)	C(1)–O(1)	1.119(16)	C(45)–C(46)	1.414(17)	C(92)–C(93)	1.373(21)
C(2)–O(2)	1.127(16)	C(11)–C(12)	1.381(12)	C(92)–N(91)	1.319(14)	C(93)–C(94)	1.315(21)
C(11)–C(16)	1.362(18)	C(11)–N(1)	1.441(13)	C(94)–C(95)	1.328(19)	C(95)–C(96)	1.424(21)
C(12)–C(13)	1.376(15)	C(13)–C(14)	1.374(19)	C(96)–C(97)	1.431(16)	C(96)–N(91)	1.350(16)
C(14)–C(15)	1.380(14)	C(14)–C(17)	1.524(15)	C(97)–C(98)	1.382(18)	C(97)–N(9c)	1.365(18)
C(15)–C(16)	1.391(16)	C(21)–C(22)	1.364(16)	C(98)–C(99)	1.313(19)	C(99)–C(9a)	1.369(23)
C(21)–C(26)	1.390(13)	C(21)–N(3)	1.429(13)	C(9a)–C(9b)	1.403(19)	C(9b)–N(9c)	1.342(15)
C(22)–C(23)	1.414(15)	C(23)–C(24)	1.395(14)	C(999)–Cl(1)	1.669(21)	C(999)–Cl(2)	1.638(20)
C(24)–C(25)	1.342(17)	C(24)–C(27)	1.536(16)	N(1)–N(2)	1.293(10)	N(2)–N(3)	1.311(13)
C(25)–C(26)	1.413(15)	C(31)–C(32)	1.372(16)	N(4)–N(5)	1.291(12)	N(5)–N(6)	1.303(11)
C(31)–C(36)	1.369(12)	C(31)–N(4)	1.419(12)	B–F(1)	1.255(24)	B–F(2)	1.286(23)
C(32)–C(33)	1.400(15)	C(33)–C(34)	1.356(13)	B–F(3)	1.234(33)	B–F(4)	1.384(31)
C(34)–C(35)	1.353(17)	C(34)–C(37)	1.517(17)				
Rh(2)–Rh(1)–C(1)	98.0(3)	Rh(2)–Rh(1)–C(2)	100.9(3)	Rh(1)–N(1)–N(2)	129.0(7)	C(11)–N(1)–N(2)	111.9(9)
C(1)–Rh(1)–C(2)	89.6(5)	Rh(2)–Rh(1)–N(1)	80.3(2)	N(1)–N(2)–N(3)	115.8(9)	Rh(2)–N(3)–C(21)	122.9(7)
C(1)–Rh(1)–N(1)	91.1(4)	C(2)–Rh(1)–N(1)	178.4(4)	Rh(2)–N(3)–N(2)	123.7(6)	C(21)–N(3)–N(2)	112.8(9)
Rh(2)–Rh(1)–N(4)	82.9(2)	C(1)–Rh(1)–N(4)	178.4(4)	Rh(1)–N(4)–C(31)	123.0(6)	Rh(1)–N(4)–N(5)	124.0(6)
C(2)–Rh(1)–N(4)	91.5(5)	N(1)–Rh(1)–N(4)	87.7(4)	C(31)–N(4)–N(5)	112.2(9)	N(4)–N(5)–N(6)	115.4(9)
Rh(1)–Rh(2)–N(3)	85.2(2)	Rh(1)–Rh(2)–N(6)	81.6(2)	Rh(2)–N(6)–C(41)	118.9(6)	Rh(2)–N(6)–N(5)	128.4(7)
N(3)–Rh(2)–N(6)	86.4(4)	Rh(1)–Rh(2)–N(91)	99.4(2)	C(41)–N(6)–N(5)	112.7(9)	Rh(2)–N(91)–C(92)	125.4(9)
N(3)–Rh(2)–N(91)	97.8(4)	N(6)–Rh(2)–N(91)	175.8(3)	Rh(2)–N(91)–C(96)	113.3(8)	C(92)–N(91)–C(96)	121.3(11)
Rh(1)–Rh(2)–N(9c)	95.1(2)	N(3)–Rh(2)–N(9c)	177.5(4)	Rh(2)–N(9c)–C(97)	114.5(7)	Rh(2)–N(9c)–C(9b)	124.9(9)
N(6)–Rh(2)–N(9c)	96.1(4)	N(91)–Rh(2)–N(9c)	79.7(4)	C(97)–N(9c)–C(9b)	120.1(11)		
Rh(1)–C(1)–O(1)	177.9(9)	Rh(1)–C(2)–O(2)	177.5(9)				

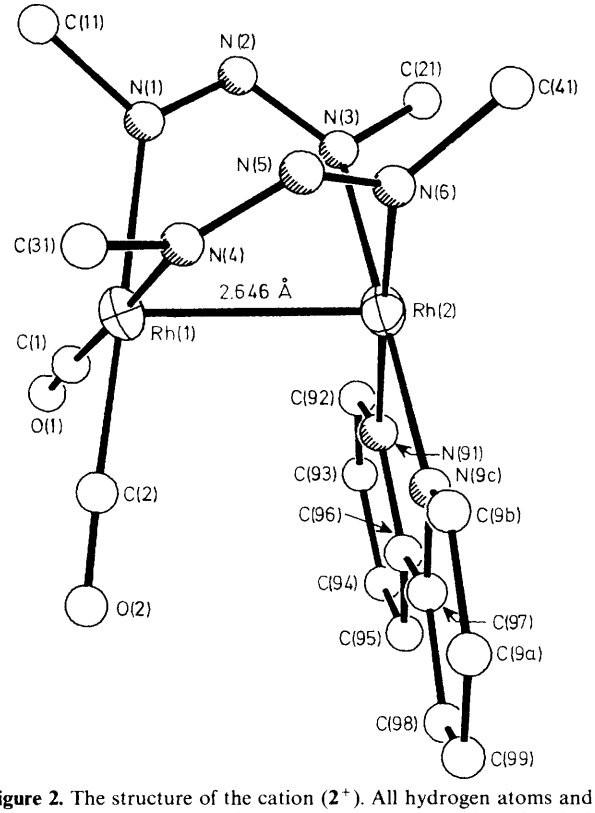

Figure 2. The structure of the cation (2^+). All hydrogen atoms and all but the *ipso* carbon atoms of the *p*-tolyl groups are omitted for clarity

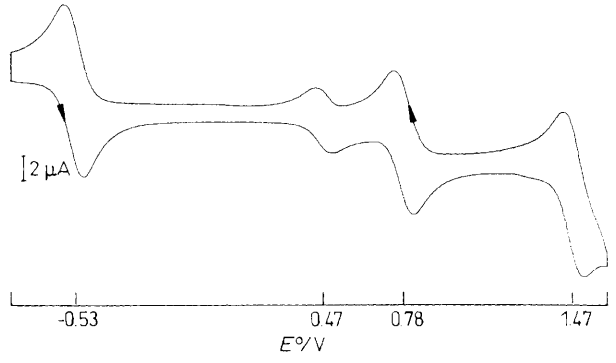

Figure 3. The cyclic voltammogram from −0.8 to +1.6 V, of $[Rh_2(CO)(PPh_3)(bipy)(\mu\text{-}RNNNR)_2]^+$ (3^+; L = PPh_3) in CH_2Cl_2 at a platinum-bead electrode. The reversible wave centred at 0.47 V is due to $[Fe(\eta\text{-}C_5H_5)_2]$, added as internal calibrant

wave of ferrocene measured under the same conditions.* Thirdly, and where comparable (*i.e.* for the $[Rh_2]^{2+}$–$[Rh_2]^{3+}$ and $[Rh_2]^{3+}$–$[Rh_2]^{4+}$ couples), the redox potentials are considerably more negative for the iodide complex.

For synthetic purposes, the third difference is the most significant in that complex (**4**) is readily oxidised to an *isolable* $[Rh_2]^{4+}$-containing complex (**A**); the other differences between the c.v.s of (3^+) and (**4**) are further discussed below in the light of the full characterisation of (**A**).

The reaction of $[Fe(\eta\text{-}C_5H_5)_2][PF_6]$ with (**4**) in CH_2Cl_2 readily gave the black crystalline material (**A**) which had an elemental analysis (C, H, and N), i.r. carbonyl spectrum (Table 1), and ^1H n.m.r. spectrum† in agreement with the formation

* For example, at a scan rate of 200 mV s^{-1} and a concentration of 5 × 10^{-4} mol dm^{-3}, Δ(ferrocene) = 80 mV, and Δ for the reduction and three oxidation waves of (**4**) are 85, 160, 75, and 80 mV respectively.

† The ^1H n.m.r. spectrum (in CD_3NO_2) is complex in the regions associated with the bipy ligand and *p*-C_6H_4 substituents, but the observation of four methyl resonances at δ 2.46, 2.37, 2.22, and 2.16 is in agreement with a highly asymmetric structure; the presence of CH_2Cl_2 as solvent of crystallisation was also confirmed.

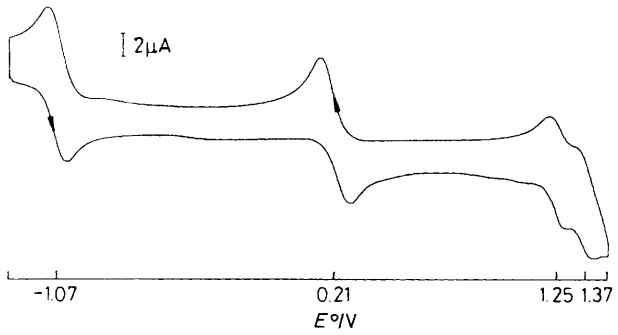

Figure 4. The cyclic voltammogram, from −1.3 to +1.5 V, of $[Rh_2I(CO)(bipy)(\mu\text{-}RNNNR)_2]$ (**4**) in CH_2Cl_2 at a platinum-bead electrode

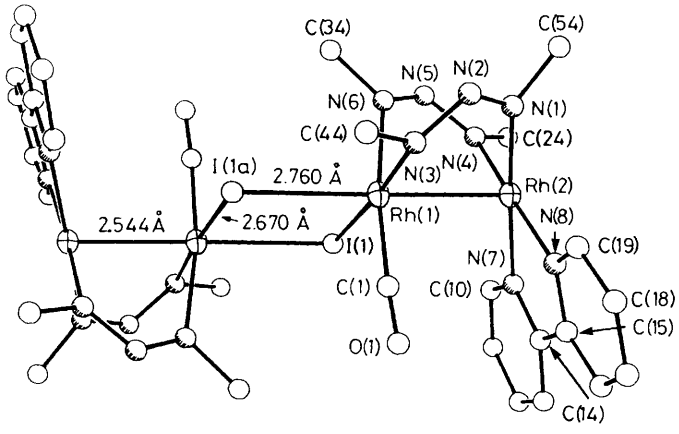

Figure 5. The structure of the dication of $[\{Rh_2(\mu\text{-}I)(CO)(bipy)(\mu\text{-}RNNNR)_2\}_2][PF_6]_2$ (**5**). All hydrogen atoms and all but the *ipso* carbon atoms of the *p*-tolyl groups are omitted for clarity

of the diamagnetic $[PF_6]^-$ salt of (4^+). In addition, the c.v. of the product was identical to that of (**4**) except that the wave at 0.21 V was due to a reduction process (once again confirmed by voltammetry at a rotating platinum electrode). Surprisingly, however, an *X*-ray structural study on (**A**), as its CH_2Cl_2 solvate, has shown it to be a dimer of (4^+), namely $[\{Rh_2I(CO)(bipy)(\mu\text{-}RNNNR)\}_2][PF_6]_2$ (**5**).

The structure of the tetranuclear dication of (**5**) is shown in Figure 5, and selected bond lengths and angles are listed in Table 4. The dication has crystallographically imposed $\bar{1}$ (C_i) symmetry with two iodine atoms bridging the two $[Rh_2]^{4+}$ units. The Rh–(μ-I) distances are not symmetric, that *trans* to the Rh ··· Rh vector within an Rh_2 unit being longer than that in the *cis* position [*i.e.* Rh(1)–I(1a) 2.760(1), Rh(1)–I(1) 2.670(1) Å]. Rather weak co-ordination of ligands in the axial site of $[Rh_2]^{4+}$ species {notably $[Rh_2(O_2CR)_4L_2]$ complexes} has been observed previously.[6] The Rh(1)–Rh(2) distance [2.544(1) Å] is considerably shorter than the Rh ··· Rh distances in (2^+) and $[Rh_2(CO)_2(PPh_3)_2(\mu\text{-}RNNNR)_2]^Z$ (Z = 0 or 1) reflecting the higher Rh–Rh bond order in (**5**) (formally 1 compared with 0.5 in $[Rh_2]^{3+}$ and 0 in $[Rh_2]^{2+}$ species). The Rh–Rh bond in (**5**) is however rather longer than in the majority of $[Rh_2]^{4+}$ species in which the Rh–Rh vector is tetrabridged, as in the tetrakis(carboxylates) for example.[6] The Rh ··· Rh distance bridged by the two μ-I ligands is non-bonding, at 4.099(1) Å. As in (2^+), the rhodium atoms show near planar four-co-ordination (ignoring Rh ··· Rh and axial Rh ··· I contacts) by the μ-RNNNR, CO, bipy, and iodine ligands. These planes are tilted by 19.9° relative to one another, less than in the $[Rh_2]^{3+}$ cases (22.3 and 31.3°) and the $[Rh_2]^{2+}$ case (40.8°, see above), but still well above the value of 0° which is observed in $[Rh_2(O_2CR)_4]$ complexes where the Rh_2 unit is tetrabridged. The planarity at Rh(1) is notably distorted [root mean square (r.m.s.) displacement from the mean plane through Rh(1), I(1), C(1), N(3), and N(6) is 0.093 Å, *cf.* 0.023 Å for the Rh(2) plane, and 0.009 and 0.007 Å for corresponding planes in (2^+)], and, in addition, the displacement of Rh(1) from the plane is away from Rh(2) (by 0.052 Å). In contrast, Rh(2) is displaced 0.030 Å towards Rh(1) from its plane [*cf.* displacements of 0.017 and 0.006 Å towards the second metal in (2^+)]. Taken with the longer than usual Rh–Rh bond in (**5**), these distortions indicate that the axial Rh(1)–I(1a) interaction disrupts the Rh(1)–Rh(2) bonding to some extent, and that dimerisation distorts the planar co-ordination at Rh(1). As usual the $Rh_2(\mu\text{-}NNN)_2$ unit is twisted to show local C_2 rather than C_{2v} symmetry but by a larger amount than for the $[Rh_2]^{3+}$ and $[Rh_2]^{2+}$ species [N–Rh–Rh–N torsion angles −27.7 and −26.6° in (**5**)].

In the light of the structural study on complex (**5**), further qualitative comments can be made on the c.v. of (**4**) [and also on that of (**5**), of course]. First, the increase in the peak separation for the wave associated with the oxidation of (**4**) is most probably related to the reversible dimerisation process which gives (**5**); *i.e.* the wave does not relate simply to a diffusion-controlled reversible one-electron transfer but rather to the overall sequence shown in Scheme 2. Clearly, more detailed

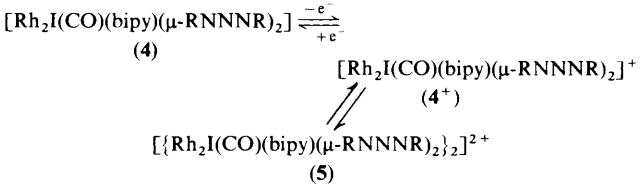

Scheme 2. R = *p*-tolyl

studies are required, particularly in order to quantify the kinetics and thermodynamics of the dimerisation step.

Secondly, the second and third oxidation waves in the c.v. of (**4**), at 1.24 and 1.39 V, are due to the oxidation of (**5**) to (5^+) and (5^{2+}), possibly involving sequential loss of one electron from each of the two $[Rh_2]^{4+}$-containing centres, and formally giving species with $[Rh_4]^{9+}$ and $[Rh_4]^{10+}$ cores. Clearly, these waves should be half the height of the other waves in the c.v. of (**4**), as observed.

Other examples of $[Rh_2]^{4+}$-containing complexes with a ligand bound to one of the axial sites (*i.e. trans* to the Rh–Rh bond) can be prepared from (**2**), (3^+), (**4**), or (**5**). Thus, the dimeric dication (**5**) undergoes iodide-bridge cleavage with iodide ion to give the black, monomeric complex $[Rh_2I_2(CO)(bipy)(\mu\text{-}RNNNR)_2]$ (**6**) (Table 1). The ^1H n.m.r. spectrum is again complex, but the observation of four methyl resonances ($[^2H_8]$toluene; δ 2.16, 2.15, 1.96, and 1.95) for the *p*-tolyl substituents of the triazenide bridges is consistent with the structure shown in Scheme 1 rather than that in which the carbonyl ligand is axially bound and the two iodine atoms are *trans* to triazenide nitrogens.

Complex (**6**) can also be made directly from (**2**) and iodine, *i.e. via* the oxidative addition of the halogen to one of the metals of the binuclear unit. This reaction is unusual in that the addition of I_2 to other, related dirhodium and di-iridium complexes, for example $[\{Rh(CO)_2(\mu\text{-}L')\}_2]$ [L = RNNNR[7] or PhNC(Ph)NPh[8]], $[\{M(CO)L(\mu\text{-}pz)\}]$ (pz = pyrazolyl; M = Rh, L = CO;[9] M = Ir, L = PPh_3[10]), $[Rh_2(CO)_2(PPh_3)_2\{\mu\text{-}1,8\text{-}(NH)_2C_{10}H_6\}]$,[11] $[\{Ir(CO)_2(\mu\text{-}2\text{-}SC_5H_4N)\}_2]$,[12] and $[Ir_2(NO)(\eta^4\text{-}cod)_2(\mu\text{-}pz)_2]^+$ (cod = cyclo-octa-1,5-diene)[13]

Table 4. Selected bond lengths (Å) and angles (°) for the complex (**5**)·2.5CH_2Cl_2

Rh(1)–I(1)	2.670(1)	Rh(1)–Rh(2)	2.544(1)	C(16)–C(17)	1.368(10)	C(15)–C(16)	1.366(10)
Rh(1)–N(3)	2.065(4)	Rh(1)–N(6)	2.105(5)	C(18)–C(19)	1.371(10)	C(17)–C(18)	1.379(12)
Rh(1)–C(1)	1.858(6)	Rh(1)–I(1a)	2.760(1)	C(21)–C(22)	1.393(9)	C(20)–C(21)	1.504(10)
Rh(2)–N(4)	2.012(5)	Rh(2)–N(1)	2.027(5)	C(22)–C(23)	1.377(9)	C(21)–C(26)	1.379(9)
Rh(2)–N(8)	2.054(5)	Rh(2)–N(7)	2.063(5)	C(24)–C(25)	1.394(8)	C(23)–C(24)	1.379(8)
P(1)–F(2)	1.543(6)	P(1)–F(1)	1.578(7)	C(30)–C(31)	1.535(13)	C(25)–C(26)	1.386(10)
P(1)–F(4)	1.556(7)	P(1)–F(3)	1.579(6)	C(31)–C(36)	1.367(13)	C(31)–C(32)	1.382(13)
P(1)–F(6)	1.587(5)	P(1)–F(5)	1.552(6)	C(33)–C(34)	1.378(10)	C(32)–C(33)	1.395(11)
N(1)–C(54)	1.424(6)	N(1)–N(2)	1.295(7)	C(35)–C(36)	1.370(12)	C(34)–C(35)	1.384(11)
N(4)–C(24)	1.427(7)	N(4)–N(5)	1.305(7)	C(41)–C(42)	1.374(12)	C(40)–C(41)	1.526(12)
N(7)–C(14)	1.348(8)	N(7)–C(10)	1.359(7)	C(42)–C(43)	1.393(11)	C(41)–C(46)	1.375(13)
N(8)–C(19)	1.340(7)	N(8)–C(15)	1.353(8)	C(44)–C(45)	1.382(9)	C(43)–C(44)	1.374(11)
N(3)–C(44)	1.437(8)	N(2)–N(3)	1.304(5)	C(50)–C(51)	1.509(8)	C(45)–C(46)	1.389(10)
N(6)–C(34)	1.431(9)	N(5)–N(6)	1.307(6)	C(51)–C(56)	1.357(11)	C(51)–C(52)	1.380(12)
C(10)–C(11)	1.375(10)	O(1)–C(1)	1.126(8)	C(53)–C(54)	1.372(8)	C(52)–C(53)	1.407(8)
C(12)–C(13)	1.384(10)	C(11)–C(12)	1.375(11)	C(55)–C(56)	1.374(7)	C(54)–C(55)	1.380(10)
C(14)–C(15)	1.464(8)	C(13)–C(14)	1.388(10)				
I(1)–Rh(1)–Rh(2)	99.2(1)	I(1)–Rh(1)–N(3)	175.0(1)	F(1)–P(1)–F(5)	89.8(3)	F(2)–P(1)–F(5)	93.6(4)
Rh(2)–Rh(1)–N(3)	82.3(1)	I(1)–Rh(1)–N(6)	86.2(1)	F(3)–P(1)–F(5)	89.1(4)	F(4)–P(1)–F(5)	91.7(3)
Rh(2)–Rh(1)–N(6)	82.0(1)	N(3)–Rh(1)–N(6)	89.3(2)	F(1)–P(1)–F(6)	87.1(3)	F(2)–P(1)–F(6)	91.3(3)
I(1)–Rh(1)–C(1)	91.3(2)	Rh(2)–Rh(1)–C(1)	88.9(2)	F(3)–P(1)–F(6)	85.9(3)	F(4)–P(1)–F(6)	91.1(3)
N(3)–Rh(1)–C(1)	93.5(2)	N(6)–Rh(1)–C(1)	170.1(2)	F(5)–P(1)–F(6)	174.2(4)	Rh(2)–N(1)–N(2)	124.6(3)
I(1)–Rh(1)–I(1a)	82.0(1)	Rh(2)–Rh(1)–I(1a)	178.8(1)	Rh(2)–N(1)–C(54)	122.0(4)	N(2)–N(1)–C(54)	113.4(5)
N(3)–Rh(1)–I(1a)	96.6(1)	N(6)–Rh(1)–I(1a)	97.8(1)	Rh(2)–N(4)–N(5)	125.1(4)	Rh(2)–N(4)–C(24)	121.0(4)
C(1)–Rh(1)–I(1a)	91.4(2)	Rh(1)–I(1)–Rh(1a)	98.0(1)	N(5)–N(4)–C(24)	113.8(5)	Rh(2)–N(7)–C(10)	125.9(4)
Rh(1)–Rh(2)–N(1)	81.6(1)	Rh(1)–Rh(2)–N(4)	82.8(1)	Rh(2)–N(7)–C(14)	114.7(4)	C(10)–N(7)–C(14)	119.4(5)
N(1)–Rh(2)–N(4)	87.7(2)	Rh(1)–Rh(2)–N(7)	100.3(1)	Rh(2)–N(8)–C(15)	115.5(4)	Rh(2)–N(8)–C(19)	125.6(4)
N(1)–Rh(2)–N(7)	174.0(2)	N(4)–Rh(2)–N(7)	98.1(2)	C(15)–N(8)–C(19)	118.8(5)	N(1)–N(2)–N(3)	115.3(5)
Rh(1)–Rh(2)–N(8)	100.8(1)	N(1)–Rh(2)–N(8)	95.0(2)	Rh(1)–N(3)–N(2)	119.2(4)	Rh(1)–N(3)–C(44)	122.2(3)
N(4)–Rh(2)–N(8)	175.7(2)	N(7)–Rh(2)–N(8)	79.1(2)	N(2)–N(3)–C(44)	114.4(5)	N(4)–N(5)–N(6)	115.0(5)
F(1)–P(1)–F(2)	89.1(4)	F(1)–P(1)–F(3)	89.4(4)	Rh(1)–N(6)–N(5)	120.1(4)	Rh(1)–N(6)–C(34)	125.6(3)
F(2)–P(1)–F(3)	176.9(4)	F(1)–P(1)–F(4)	176.8(3)	N(5)–N(6)–C(34)	111.0(5)	Rh(1)–C(1)–O(1)	176.0(4)
F(2)–P(1)–F(4)	93.6(4)	F(3)–P(1)–F(4)	87.8(4)				

occurs across the two metals, *i.e.* to give products with I–M–M–I (M = Rh or Ir) skeletons.

The isolation of (2^+), (**4**), (**5**), and (**6**) suggests an e.c.e.c. (e.c. = electrochemical–chemical) mechanism (Scheme 3) for the oxidative addition of I_2 to (**2**), *i.e.* one involving sequential

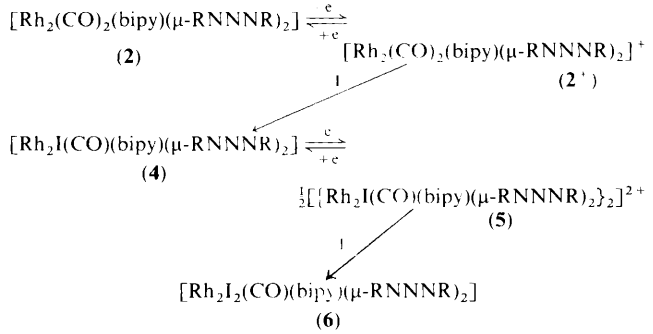

Scheme 3. An e.c.e.c. mechanism for the oxidative addition of I_2 to complex (**2**) to give (**6**); R = *p*-tolyl

one-electron oxidation steps rather than a concerted two-electron process; we have previously postulated[14] a similar mechanism for the formation of $[FeI_2(CO)_3(PPh_3)]$ from $[Fe(CO)_3(PPh_3)_2]$ and iodine although in that case conclusive evidence for all the suggested intermediates was not obtained. Clearly, the strengthening of the metal–metal interaction as the oxidation state of the $[Rh_2]^{Z+}$ core is increased is a factor in the stabilisation of the intermediates in the binuclear system. Effectively, the formation of (**6**) from (**2**) involves oxidative addition at one metal centre mediated by the second.

Although the mechanism shown in Scheme 3 is plausible, additional (or alternative) steps are possible. For example, the reaction between (2^+) and iodine gives (**5**) directly. It is interesting to note an intermediate in this particular reaction, showing two carbonyl bands in the i.r. spectrum at 2 121 and 2 089 cm^{-1}. The most likely identity for this species is $[Rh_2I(CO)_2(bipy)(\mu\text{-RNNNR})_2]^+$, and bubbling CO through a solution of (4^+) results in the observation of the same i.r. spectrum. This intermediate could not be isolated but its formation indicates that axial co-ordination is the most likely first step in the carbonyl displacement reaction of (2^+), *i.e.* substitution occurs *via* an associative mechanism.

The reactions of (**5**) with $Na[S_2CNMe_2]$, and of [3^+; L = PPh_3 or $P(OPh)_3$] with $[N(CH_2Ph)Et_3]Cl$ in the presence of $[Fe(\eta\text{-}C_5H_5)_2][PF_6]$, provide two more examples of axially co-ordinated $[Rh_2]^{4+}$ complexes, namely the green, diamagnetic, air-stable solids $[Rh_2(CO)(S_2CNMe_2)(bipy)(\mu\text{-RNNNR})_2][PF_6]$ (**7**) and $[Rh_2Cl(CO)L(bipy)(\mu\text{-RNNNR})_2][PF_6]$ [**8**; L = PPh_3 or $P(OPh)_3$]; the latter are related to the proposed intermediate $[Rh_2I(CO)_2(bipy)(\mu\text{-RNNNR})_2]^+$, noted above.

Which of the ligands CO, L, or Cl is in the axial position of (**8**) cannot be defined by spectroscopic methods (and all attempts to obtain crystals suitable for an *X*-ray structural study failed). However, the ^1H n.m.r. spectrum of (**7**) shows five methyl resonances ($CDCl_3$; δ 3.01, 2.75, 2.38, 2.26, and 2.24; 1:1:1:1:2 ratio) which can only arise if the dithiocarbamate ligand spans the axial and one of the equatorial sites (Scheme 1).

The c.v.s of (**7**) and (**8**) show that each complex undergoes reversible one-electron oxidation and reduction (Table 2) although all attempts to generate chemically the $[Rh_2]^{5+}$ and $[Rh_2]^{3+}$ products have been unsuccessful. It is noteworthy that Δ, the difference between the potentials associated with the $[Rh_2]^{3+}$–$[Rh_2]^{4+}$ and $[Rh_2]^{4+}$–$[Rh_2]^{5+}$ couples is much

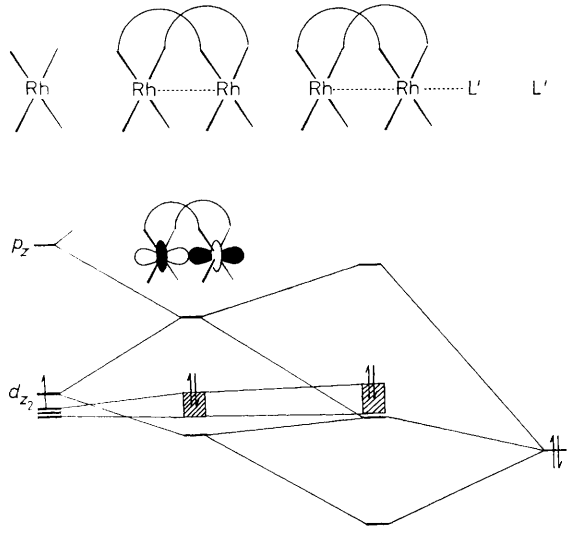

Figure 6. Schematic orbital correlation diagram for the formation of a $[Rh_2]^{4+}$ dimer $[(RhL_4)_2]$ and an axially ligated adduct, $[(RhL_4)_2L']$. The shaded block represents the set of molecular orbitals arising from overlap of the d_{xy}, d_{xz}, and d_{yz} orbitals (Rh ··· Rh being taken as the z axis). Orbital occupancies indicated refer to rhodium(II) species

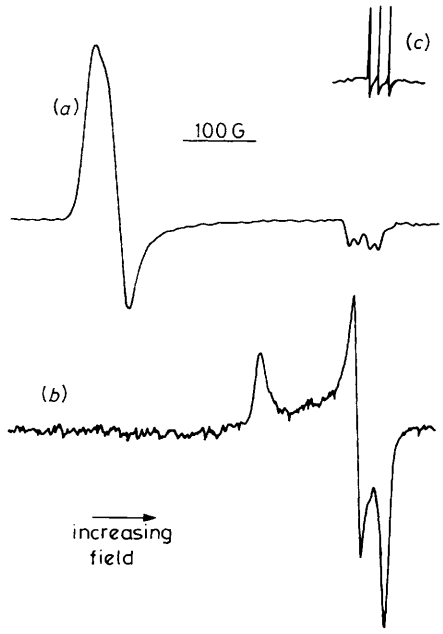

Figure 7. (*a*) The e.s.r. spectrum of $[Rh_2(CO)(PPh_3)(bipy)(\mu\text{-}RNNNR)_2][PF_6]$ (3^+; L = PPh_3) in CH_2Cl_2–1,2-dichloroethane (1:1) at −110 °C at 1.1×10^{-2} mol dm^{-3}; (*b*) as (*a*) but at 1.5×10^{-4} mol dm^{-3} concentration and in the presence of oxygen; (*c*) the e.s.r. spectrum of $K_2[NO(SO_3)_2]$ (Fremy's salt) as standard (g = 2.0057)

greater for (**7**) and (**8**) (*ca.* 1.9 V) than for those species in Table 2 which do not contain an axially bound ligand [*e.g.* for (**3**; L = PPh_3), Δ = 0.69 V].

We have previously suggested that the highest occupied molecular orbital (h.o.m.o.) of the $[Rh_2]^{2+}$ species is the Rh–Rh σ* orbital,[5] primarily composed of metal d_{z^2}, where the z axis is perpendicular to the local rhodium co-ordination plane. By implication this orbital is singly occupied (*i.e.* is the s.o.m.o.) in $[Rh_2]^{3+}$ species and is the lowest unoccupied (l.u.m.o.) in $[Rh_2]^{4+}$ species. This is in accord with the accepted picture of the electronic structure of the much-studied $[Rh_2]^{4+}$ complexes $[Rh_2(O_2CR)_4L_2]$.[6] This orbital would be expected to act as the site of nucleophilic attack when partly or completely unoccupied, thereby leading, for example, to associative substitution reactions. We have confirmed the nature of this orbital by extended-Hückel m.o. calculations on a model compound $[Rh_2(CO)_4(\mu\text{-}HNNNH)_2]$.[15] In this light the effect of co-ordinating an extra, axial ligand, *e.g.* as in (**7**) and (**8**), on Δ may be understood. Figure 6 shows in a schematic way the development of the relevant orbitals. The interaction of the ligand (L') lone pair with the d_{z^2} orbital will cause destabilisation of the σ* orbital, the l.u.m.o. of the $[Rh_2]^{4+}$ species, as it forms Rh–L' bonding and antibonding orbitals. In contrast the h.o.m.o. of these complexes is one of a block of Rh *d* orbitals, largely unaffected by the approach of an axial ligand being of π or δ symmetry with respect to the Rh–L' bond. As a result the ease of oxidation of $[Rh_2]^{4+}$ species would be expected to be rather insensitive to axial ligation by L', whereas $[Rh_2]^{3+}$ species should be more readily oxidised when L' is bound than when it is absent. This is entirely in accord with the observed values of Δ.

The E.S.R. Spectra of the $[Rh_2]^{3+}$*-containing Complexes* (2^+), (3^+), *and* (**4**).—At room temperature, each of the $[Rh_2]^{3+}$-containing complexes (2^+), [3^+; L = PPh_3 or $P(OPh)_3$], and (**4**) shows a broad, single-line resonance at *ca.* g = 2.16—2.18 (Table 5), similar to those of $[\{Rh(CO)(PPh_3)(\mu\text{-}RNNNR)\}_2]^+$ and related Lewis-base and η^4-diene derivatives.[2] At lower temperatures, however, the well resolved anisotropic spectra of the bipy complexes show the presence of two paramagnetic species. Our preliminary studies suggested[4] that the relative abundance of the two species was dependent on the total overall concentration; Figure 7(*a*) and (*b*) show the spectra obtained for (3^+; L = PPh_3) in a CH_2Cl_2–CH_2ClCH_2Cl (1:1) glass at −110 °C at 1.1×10^{-2} and 1.5×10^{-4} mol dm^{-3} concentration respectively. However, it is now clear that the spectra obtained at the lower concentration are more likely due to the formation of a superoxide complex when the $[Rh_2]^{3+}$-containing species reacts with adventitious oxygen.

Bear *et al.*[16] have recently shown that $[Rh_2(ap)_4]$ (ap = 2-anilinopyridinate) binds molecular oxygen to give an $Rh^{II}Rh^{III}(O_2^-)$ superoxide adduct which can be reduced to the superoxide-containing anion $[Rh_2(ap)_4(O_2)]^-$. The anisotropic e.s.r. spectrum of $[Rh_2(ap)_4(O_2)]^-$ in CH_2Cl_2 (g_1 = 2.094, g_2 = 2.026, g_3 = 1.998; $g_{av.}$ = 2.039) is remarkably similar to that shown in Figure 7(*b*) (g_1 = 2.084, g_2 = 2.010, g_3 = 1.992; $g_{av.}$ = 2.029) suggesting strongly that the latter is also due to superoxide co-ordination to an $[Rh_2]^{4+}$ core.

Although Bear and Kadish's compound is an axial adduct, preliminary studies suggest[17] that complex (2^+) undergoes carbonyl substitution with O_2. Thus, addition of molecular oxygen to a solution of the dicarbonyl cation in CH_2Cl_2 at room temperature results in a strong e.s.r. singlet signal at g = 2.011, and an i.r. carbonyl spectrum showing only one absorption, at 2 070 cm^{-1}. Further studies are in progress.

The spectra observed at the higher concentrations (Table 5) are very similar to all of those so far reported for other $[Rh_2]^{3+}$-containing complexes, for example the Lewis-base and η^4-diene derivatives of $[\{Rh(CO)_2(\mu\text{-}RNNNR)\}_2]^+$ referred to above,[2] $[Rh_2(\mu\text{-}O_2CMe)_4]^-$,[18] $[Rh_2\{\mu\text{-}PhNC(Ph)NPh\}_4]^-$,[19] $[Rh_2(\mu\text{-}Ph_2PCH_2PPh_2)_2(dimen)_2]^{3+}$ (dimen = 1,8-di-isocyanomenthane),[20] and $[Rh_2(\eta^4\text{-}cod)_2(\mu\text{-}L')_2]^+$ (L' = 3,5-dimethylpyrazolyl).[21] In common with these species, the e.s.r. spectra of the bipy complexes show hyperfine coupling to ^{103}Rh, most obviously on the $g_{\|}$ component (*ca.* 2.00) but also on the other g components of (**4**) (Table 5).* However, in none of

* A quantitative analysis of the e.s.r. spectra of $[Rh_2]^{3+}$-containing triazenide complexes, including the bipy complexes described herein, is nearing completion and will be reported elsewhere (P. H. Rieger, Brown University, Providence, Rhode Island, U.S.A., unpublished work).

Table 5. The e.s.r. spectra of $[Rh_2]^{3+}$ complexes and $[Rh_2]^{4+}$ superoxides

Complex	g_1	g_2	g_3	$g_{av.}$	$A(^{103}Rh)$/G	Medium	Temperature/°C
(**2**$^+$)				2.179		CH_2Cl_2	20
	2.279	2.242	2.002	2.174		Powder	20
	2.260	2.233	2.002	2.165	32,10[a]	CH_2Cl_2–thf (1:2)	−140
	2.082	2.021	1.988	2.030[b]		CH_2Cl_2–thf (1:2)	−140
	2.272	2.243	2.000	2.172	31[c]	CH_2Cl_2–CH_2ClCH_2Cl (1:1)	−110
	2.084	2.009	1.988	2.027[b]		CH_2Cl_2–CH_2ClCH_2Cl (1:1)	−110
(**3**$^+$; L = PPh_3)				2.179		thf	20
	2.082	2.009	1.986	2.026[b]		thf	−196
	2.087	2.008	1.998	2.031[b]		CH_2Cl_2–thf (1:2)	−140
	2.276	2.241	2.006	2.174	28,12[d]	CH_2Cl_2–CH_2ClCH_2Cl (1:1)	−110
	2.084	2.010	1.992	2.029[b]		CH_2Cl_2–CH_2ClCH_2Cl (1:1)	−110
[**3**$^+$; L = $P(OPh)_3$]				2.177		CH_2Cl_2	20
(**4**)				2.159		CH_2Cl_2	20
				2.158		thf	20
	2.088	2.009	1.990	2.029[b]		thf	−196
	2.250	2.196	2.022	2.156	15,18,28[e]	CH_2Cl_2–thf (1:2)	−140
	2.086	2.009	1.990	2.029[b]		CH_2Cl_2–thf (1:2)	−140

[a] Hyperfine coupling of doublet at g_3 = 2.002. [b] Superoxide complex, see text. [c] Hyperfine coupling of doublet at g_3 = 2.000; second coupling unresolved. [d] Hyperfine coupling of doublet of doublets at g_3 = 2.006. [e] A_1 (doublet), A_2 (triplet), A_3 (doublet) respectively

these other cases has evidence for superoxide adduct formation been described.

Conclusions

The incorporation of bipy into the redox-active unit $[\{Rh(CO)_2(\mu\text{-RNNNR})\}_2]$ has given $[Rh_2(CO)_2(bipy)(\mu\text{-RNNNR})_2]$ (**2**), the precursor to a wide range of isolable, asymmetric, $[Rh_2]^{2+}$-, $[Rh_2]^{3+}$-, and $[Rh_2]^{4+}$-containing complexes. Of particular interest is the isolation of all the intermediates postulated in an e.c.e.c. mechanism for the oxidative addition of I_2 to (**2**).

Experimental

The preparation, purification, and reactions of the complexes were carried out under an atmosphere of dry nitrogen; i.r. spectroscopy was generally used to monitor the course of the reactions. Unless otherwise stated products (*i*) were purified by dissolution in CH_2Cl_2, filtration, addition of n-hexane, and partial evaporation of the solvent mixture *in vacuo* to induce precipitation, and (*ii*) are air stable, dissolving in polar solvents such as CH_2Cl_2 or tetrahydrofuran (thf) to give solutions which slowly decompose in air. The compounds $[\{Rh(CO)_2(\mu\text{-RNNNR})\}_2]$,[2] $[Fe(\eta\text{-}C_5H_5)_2][PF_6]$,[22] and $[N_2C_6H_4F\text{-}p][PF_6]$[23] were prepared by published methods.

Infrared spectra were recorded on a Nicolet MX-5 FT spectrometer, or a Perkin-Elmer PE257 spectrometer with calibration against the absorption band of polystyrene at 1 601 cm^{-1}. Hydrogen-1 n.m.r. spectra were recorded on a JEOL PMX60 instrument and calibrated against $SiMe_4$ as internal reference. *X*-Band e.s.r. spectra were recorded on a Varian Associates 4502/15 instrument and were calibrated against a solid sample of the diphenylpicrylhydrazyl radical or a 10^{-4} mol dm^{-3} aqueous solution of $K_2[NO(SO_3)_2]$ (Fremy's salt) (5×10^{-2} mol dm^{-3} in K_2CO_3 as buffer). Electrochemical studies were carried out using an AMEL Electrochemolab instrument in conjunction with a three-electrode cell. For cyclic voltammetry the working electrode was a platinum bead, the auxiliary electrode a platinum wire, and the reference an aqueous saturated calomel electrode (s.c.e.) separated from the test solution by a fine-porosity frit and an agar bridge saturated with KCl. Voltammetry used a platinum-bead electrode rotated at 600 revolutions min^{-1}. Solutions were 0.5×10^{-3} mol dm^{-3} in complex and 0.1 mol dm^{-3} in $[NBu^n_4][PF_6]$ as supporting electrolyte. After cyclic voltammetric measurements were carried out on each complex, either $[Fe(\eta\text{-}C_5H_5)_2]$ or $[Fe(\eta\text{-}C_5Me_5)_2]$ was added to the test solution as an internal calibrant. Under the conditions described above, the E^o values of the couples $[Fe(\eta\text{-}C_5H_5)_2]^+$–$[Fe(\eta\text{-}C_5H_5)_2]$ and $[Fe(\eta\text{-}C_5Me_5)_2]^+$–$[Fe(\eta\text{-}C_5Me_5)_2]$ are 0.47 and −0.07 V respectively. Microanalyses were carried out by the staff of the Microanalytical Service of the School of Chemistry, University of Bristol.

(2,2′-Bipyridyl)dicarbonylbis[μ-(*di*-p-*tolyltriazenido*-N^1N^3)]-*dirhodium*, $[Rh_2(CO)_2(bipy)(\mu\text{-RNNNR})_2]$ (R = p-*tolyl*).—A mixture of $[\{Rh(CO)_2(\mu\text{-RNNNR})\}_2]$ (0.50 g, 0.65 mmol) and 2,2′-bipyridyl (0.135 g, 0.86 mmol) was heated under gentle reflux in n-heptane (90 cm^3) for 24 h, with the rigorous exclusion of oxygen. The resulting black crystals were washed with n-heptane, and dried *in vacuo*, yield 0.46 g (82%).

The solid is unstable in air, but can be stored under nitrogen at −10 °C for at least 10 d. The complex is soluble in benzene, CH_2Cl_2, and thf, giving dark red solutions which very rapidly become brown when exposed to air.

(2,2′-Bipyridyl)dicarbonylbis[μ-(*di*-p-*tolyltriazenido*-N^1N^3)]-*dirhodium Hexafluorophosphate*, $[Rh_2(CO)_2(bipy)(\mu\text{-RNNNR})_2][PF_6]$.—To a stirred solution of $[Rh_2(CO)_2(bipy)(\mu\text{-RNNNR})_2]$ (0.174 g, 0.2 mmol) in CH_2Cl_2 (30 cm^3) was added $[Fe(\eta\text{-}C_5H_5)_2][PF_6]$ (0.067 g, 0.2 mmol). After 2 min the resulting dark brown solution was filtered, n-hexane (30 cm^3) was added, and the mixture reduced in volume *in vacuo* to give the product as dark brown crystals, yield 0.16 g (80%).

(2,2′-Bipyridyl)carbonylbis[μ-(*di*-p-*tolyltriazenido*-N^1N^3)]-*(triphenylphosphine)dirhodium Hexafluorophosphate*, $[Rh_2(CO)(PPh_3)(bipy)(\mu\text{-RNNNR})_2][PF_6]$.—To a solution of $[Rh_2(CO)_2(bipy)(\mu\text{-RNNNR})_2][PF_6]$ (0.10 g, 0.1 mmol) in CH_2Cl_2 (20 cm^3) was added PPh_3 (0.026 g, 0.1 mmol). The brown solution was treated as above to give the brown, microcrystalline product, yield 0.11 g (89%).

The complex $[Rh_2(CO)\{P(OPh)_3\}(bipy)(\mu\text{-RNNNR})_2][PF_6]$ was prepared similarly, but was crystallised by purification from CH_2Cl_2–diethyl ether.

(2,2′-Bipyridyl)carbonyliodobis[μ-(*di*-p-*tolyltriazenido*-N^1N^3)]-*dirhodium*, $[Rh_2I(CO)(bipy)(\mu\text{-RNNNR})_2]$.—To a cold

Table 6. Crystal data, structure analysis, and refinement[a]

Compound	$(2^+)BF_4 \cdot CH_2Cl_2$	$(5) \cdot 2.5CH_2Cl_2$
Formula	$C_{41}H_{38}BCl_2F_4N_8O_2Rh_2$	$C_{81}H_{82}Cl_5F_{12}I_2N_{16}O_2P_2Rh_4P_2$
M	1 038.4	2 433.2
Crystal system	Monoclinic	Triclinic
Space group	$P2_1/n$ (no. 14)	$P\bar{1}$ (no. 2)
a/Å	20.769(4)	13.351(3)
b/Å	11.026(3)	14.005(4)
c/Å	21.648(5)	14.540(4)
α/°	90	102.28(3)
β/°	115.46(2)	110.76(3)
γ/°	90	95.30(3)
U (Å^3)	4 476(2)	2 441.8(12)
Z	4	1
D_c /g cm^{-3}	1.54	1.65
F(000)	2 084	1 180
μ/cm^{-1}	9.05	8.51
Total data	5 038	7 009
Unique data	4 585	6 675
Observed data (N_o)	3 332	5 734
Crystal faces [distance from origin (mm)]	(111) [0.11], ($\bar{1}\bar{1}\bar{1}$) [0.11], ($\bar{1}$01) [0.05], (10$\bar{1}$) [0.05], (1$\bar{1}$1) [0.11], ($\bar{1}$0$\bar{1}$) [0.10], ($\bar{1}$1$\bar{1}$) [0.11]	(001) [0.14], (00$\bar{1}$) [0.14], (100) [0.1], ($\bar{1}$00) [0.1], (010) [0.11], (0$\bar{1}$0) [0.11], (1$\bar{1}$0) [0.13], (0$\bar{1}$1) [0.15]
Minimum, maximum transmission coefficients	0.824, 0.915	0.799, 0.843
R_{merg}	0.026	0.015
Least-squares variables, N_v	361	581
R^b	0.065	0.037
R'	0.065	0.048
S	1.49	1.38
g	0.0005	0.0005
Difference map features (e Å^{-3})	+0.71, −0.79	+0.65, −0.53

[a] Details common to both compounds: T = 295 K; λ = 0.710 69 Å, graphite monochromatised; 2θ range 4—50°; scan method θ—2θ; scan width (2θ) = 2.0 + $\Delta\alpha_1\alpha_2$; observation criterion $F^2 > 3\sigma(F^2)$. [b] $R = \Sigma|\Delta|/\Sigma|F_o|$, $R' = (\Sigma w\Delta^2/\Sigma F_o^2)^{\frac{1}{2}}$, $S = [\Sigma w\Delta^2/(N_o - N_v)]^{\frac{1}{2}}$, and $\Delta = |F_o| - |F_c|$, where $w = [\sigma_c^2(F_o) + gF_o^2]^{-1}$ and $\sigma_c^2(F_o)$ is the variance in F_o based on counting statistics.

Table 7. Atomic co-ordinates (× 10^4) for complex $(2^+)BF_4 \cdot CH_2Cl_2$

Atom	x	y	z	Atom	x	y	z
Rh(1)	3 650(1)	2 174(1)	632(1)	C(46)	973(6)	2 134(10)	225(5)
Rh(2)	2 527(1)	1 698(1)	−530(1)	C(47)	−938(5)	1 209(12)	−906(7)
C(1)	4 291(6)	1 059(10)	535(5)	C(92)	3 216(6)	−144(10)	−1 088(5)
C(2)	4 077(6)	3 427(11)	359(5)	C(93)	3 539(7)	−560(13)	−1 484(6)
C(11)	3 396(5)	664(9)	1 683(5)	C(94)	3 670(7)	270(12)	−1 851(6)
C(12)	4 076(5)	1 014(9)	2 129(5)	C(95)	3 515(7)	1 443(12)	−1 874(6)
C(13)	4 288(6)	902(9)	2 822(5)	C(96)	3 176(6)	1 846(10)	−1 461(5)
C(14)	3 848(6)	415(10)	3 083(5)	C(97)	2 976(6)	3 072(10)	−1 414(5)
C(15)	3 171(6)	64(10)	2 629(5)	C(98)	3 127(6)	4 075(11)	−1 712(6)
C(16)	2 939(6)	218(10)	1 928(5)	C(99)	2 941(7)	5 166(12)	−1 609(7)
C(17)	4 106(7)	255(12)	3 852(5)	C(9a)	2 579(7)	5 366(12)	−1 218(6)
C(21)	2 022(5)	−868(10)	−425(5)	C(9b)	2 426(6)	4 347(11)	−916(6)
C(22)	2 006(6)	−1 927(10)	−105(6)	C(999)	4 378(17)	6 892(15)	951(9)
C(23)	1 549(6)	−2 874(11)	−485(6)	O(1)	4 660(4)	404(8)	456(4)
C(24)	1 127(6)	−2 767(11)	−1 187(6)	O(2)	4 320(4)	4 171(8)	171(4)
C(25)	1 144(6)	−1 718(10)	−1 493(6)	N(1)	3 186(4)	810(7)	960(4)
C(26)	1 594(6)	−756(10)	−1 122(5)	N(2)	2 732(4)	−7(7)	604(4)
C(27)	658(7)	−3 837(11)	−1 584(6)	N(3)	2 460(4)	130(7)	−62(4)
C(31)	3 184(5)	4 326(9)	1 254(5)	N(4)	2 954(4)	3 373(7)	765(4)
C(32)	2 763(6)	5 303(10)	1 225(5)	N(5)	2 270(4)	3 235(7)	495(4)
C(33)	3 003(6)	6 195(11)	1 734(5)	N(6)	2 012(4)	2 498(8)	−26(4)
C(34)	3 664(6)	6 138(11)	2 259(5)	N(91)	3 037(4)	1 003(8)	−1 083(4)
C(35)	4 099(6)	5 219(10)	2 265(5)	N(9c)	2 617(4)	3 230(8)	−1 020(4)
C(36)	3 864(6)	4 294(10)	1 762(5)	B	9 133(12)	8 147(23)	2 763(11)
C(37)	3 907(8)	7 092(12)	2 819(7)	F(1)	8 466(5)	8 068(10)	2 473(5)
C(41)	1 271(5)	2 224(9)	−232(5)	F(2)	9 410(5)	8 001(9)	3 416(5)
C(42)	855(6)	1 996(9)	−920(5)	F(3)	9 463(7)	7 526(18)	2 520(6)
C(43)	134(6)	1 648(10)	−1 129(6)	F(4)	9 276(7)	9 328(16)	2 644(8)
C(44)	−163(6)	1 557(11)	−680(6)	Cl(1)	4 148(5)	7 254(5)	135(3)
C(45)	252(6)	1 788(11)	1(6)	Cl(2)	4 521(5)	8 068(6)	1 456(4)

Table 8. Atomic co-ordinates ($\times 10^4$) for complex (**5**)·2.5CH_2Cl_2

Atom	*x*	*y*	*z*	Atom	*x*	*y*	*z*
Rh(1)	672(1)	6 241(1)	1 206(1)	C(23)	3 202(4)	5 756(4)	4 720(4)
I(1)	172(1)	4 278(1)	898(1)	C(24)	2 998(4)	5 335(4)	3 709(4)
Rh(2)	1 469(1)	6 755(1)	3 145(1)	C(25)	3 203(5)	4 381(4)	3 423(5)
P(1)	7 911(2)	1 543(1)	3 417(2)	C(26)	3 610(5)	3 884(4)	4 165(5)
F(1)	8 145(5)	911(4)	4 224(4)	C(30)	3 968(7)	5 503(9)	−1 730(6)
F(2)	6 688(4)	1 322(5)	3 221(5)	C(31)	3 529(5)	5 663(7)	−877(5)
F(3)	9 175(4)	1 797(5)	3 680(5)	C(32)	3 622(5)	4 983(6)	−302(5)
F(4)	7 744(5)	2 204(4)	2 658(4)	C(33)	3 236(5)	5 090(5)	482(5)
F(5)	7 832(6)	608(4)	2 582(4)	C(34)	2 725(4)	5 878(5)	667(4)
F(6)	8 114(5)	2 484(3)	4 334(4)	C(35)	2 630(6)	6 556(6)	87(5)
N(1)	2 409(3)	7 824(3)	2 909(3)	C(36)	3 031(6)	6 445(7)	−668(5)
N(4)	2 507(3)	5 847(3)	2 962(3)	C(40)	−446(8)	9 406(7)	−2 020(6)
N(7)	432(3)	5 781(3)	3 434(3)	C(41)	−15(7)	8 984(5)	−1 098(5)
N(8)	421(3)	7 651(3)	3 431(3)	C(42)	1 086(7)	9 086(5)	−565(6)
N(2)	2 094(4)	8 199(3)	2 135(3)	C(43)	1 496(6)	8 708(5)	279(5)
N(3)	1 170(4)	7 737(3)	1 405(3)	C(44)	794(5)	8 209(4)	590(4)
N(5)	2 830(4)	5 696(3)	2 203(3)	C(45)	−315(5)	8 134(5)	87(5)
N(6)	2 273(4)	6 023(3)	1 433(3)	C(46)	−707(6)	8 524(5)	−748(5)
O(1)	−1 477(3)	6 535(4)	1 300(4)	C(50)	6 854(5)	9 252(6)	5 658(6)
C(1)	−684(4)	6 403(4)	1 230(4)	C(51)	5 686(5)	8 903(4)	4 916(5)
C(10)	473(5)	4 806(4)	3 383(4)	C(52)	4 893(6)	8 665(4)	5 275(5)
C(11)	−292(5)	4 211(4)	3 546(4)	C(53)	3 797(5)	8 316(4)	4 607(4)
C(12)	−1 098(5)	4 611(5)	3 787(5)	C(54)	3 513(4)	8 210(4)	3 581(4)
C(13)	−1 141(5)	5 605(4)	3 846(5)	C(55)	4 313(5)	8 455(5)	3 232(5)
C(14)	−361(4)	6 174(4)	3 662(4)	C(56)	5 376(5)	8 802(5)	3 899(5)
C(15)	−357(4)	7 225(4)	3 688(4)	Cl(1)*	6 001(8)	7 623(7)	1 657(7)
C(16)	−1 071(5)	7 764(5)	3 935(5)	Cl(2)*	3 831(8)	726(9)	1 679(9)
C(17)	−1 021(6)	8 740(5)	3 919(6)	Cl(3)*	3 080(11)	1 833(9)	−477(12)
C(18)	−234(5)	9 170(5)	3 647(5)	Cl(4)*	3 953(11)	2 425(9)	1 657(14)
C(19)	470(5)	8 605(4)	3 409(4)	Cl(5)*	4 672(14)	9 045(21)	673(11)
C(20)	4 259(6)	3 744(5)	5 974(5)	C(61)*	5 507(25)	8 440(19)	−1 506(25)
C(21)	3 812(5)	4 293(5)	5 178(5)	C(62)*	6 310(27)	8 524(21)	1 274(21)
C(22)	3 608(5)	5 250(4)	5 447(4)				

* Site occupancy 0.5.

(−78 °C) solution of $[Rh_2(CO)_2(bipy)(\mu\text{-}RNNNR)_2]$ (0.2 g, 0.23 mmol) in CH_2Cl_2 (30 cm^3) was added solid iodine (0.030 g, 0.12 mmol). The solution was then allowed to warm to room temperature, n-hexane (30 cm^3) was added, and the mixture was reduced in volume *in vacuo* to give a brown precipitate. Purification from thf–n-hexane gave the product, 0.15 g (70%).

The complex is unstable in air, both in the solid state and in solution.

*Di-*μ*-iodo-bis*{(2,2′*-bipyridyl*)*carbonylbis*[μ-(*di*-p-*tolyltriazenido*-N^1N^3)]-*dirhodium*} *Bis*(*hexafluorophosphate*), $[\{Rh_2I(CO)(bipy)(\mu\text{-}RNNNR)_2\}_2][PF_6]_2$.—To a stirred solution of $[Rh_2I(CO)(bipy)(\mu\text{-}RNNNR)_2]$ (0.10 g, 0.1 mmol) in CH_2Cl_2 (20 cm^3) was added $[Fe(\eta\text{-}C_5H_5)_2][PF_6]$ (0.034 g, 0.1 mmol). After 1 min the dark brown solution was filtered, n-hexane (20 cm^3) was added, and the mixture was reduced in volume *in vacuo* to give the black, microcrystalline product, yield 0.1 g (87%).

The complex is air-stable, and soluble in CH_2Cl_2 to give a dark brown solution which only decomposes very slowly in air; the complex is insoluble in thf.

(2,2′*-Bipyridyl*)*carbonylbis*[μ-(*di*-p-*tolyltriazenido*-N^1N^3)]-*di-iododirhodium*, $[Rh_2I_2(CO)(bipy)(\mu\text{-}RNNNR)_2]$.—*Method* (*a*). To a cold (−78 °C) solution of $[Rh_2(CO)_2(bipy)(\mu\text{-}RNNNR)_2]$ (0.20 g, 0.23 mmol) in CH_2Cl_2 (20 cm^3) was added solid iodine (0.059 g, 0.23 mmol). The mixture was then allowed to warm to room temperature, n-hexane (20 cm^3) was added, and the mixture reduced in volume *in vacuo* to give the product as a brown powder, yield 0.2 g (79%).

Method (*b*). To a stirred solution of $[Rh_2I(CO)(bipy)(\mu\text{-}RNNNR)_2][PF_6]$ (0.20 g, 0.18 mmol) in CH_2Cl_2 (20 cm^3) was added $[NBu^n_4]I$ (0.067 g, 0.18 mmol). After 1 min the mixture was evaporated to dryness and the residue extracted with toluene (20 cm^3). Concentration of the extract (*ca.* 5 cm^3) and addition of n-hexane gave the product as a brown precipitate, yield 0.15 g (76%).

The complex is soluble in CH_2Cl_2, thf, and toluene and slightly soluble in diethyl ether.

(2,2′*-Bipyridyl*)*carbonyl*(*dimethyldithiocarbamato*)*bis*[μ-(*di*-p-*tolyltriazenido*-N^1N^3)]-*dirhodium Hexafluorophosphate*, $[Rh_2(CO)(S_2CNMe_2)(bipy)(\mu\text{-}RNNNR)_2][PF_6]$.—To a stirred solution of $[Rh_2I(CO)(bipy)(\mu\text{-}RNNNR)_2][PF_6]$ (0.3 g, 0.27 mmol) in CH_2Cl_2 (25 cm^3) was added $Na[S_2CNMe_2]\cdot 2H_2O$ (0.05 g, 0.28 mmol). After 20 h the mixture was filtered, n-hexane (20 cm^3) was added, and the volume of the solution was reduced *in vacuo*. The brown precipitate was then purified from CH_2Cl_2–diethyl ether to give the product as a grey-green powder, yield 0.134 g, 45%.

(2,2′*-Bipyridyl*)*carbonylchlorobis*[μ-(*di*-p-*tolyltriazenido*-N^1N^3)]-(*triphenylphosphine*)*dirhodium Hexafluorophosphate*, $[Rh_2Cl(CO)(PPh_3)(bipy)(\mu\text{-}RNNNR)_2][PF_6]$.—To a solution of $[Rh_2(CO)(PPh_3)(bipy)(\mu\text{-}RNNNR)_2][PF_6]$ (0.15 g, 0.12 mmol) in CH_2Cl_2 (25 cm^3) was added $[Fe(\eta\text{-}C_5H_5)_2][PF_6]$ (0.04 g, 0.12 mmol) and then $[N(CH_2Ph)Et_3]Cl$ (0.027 g, 0.12 mmol). The green solution was filtered, and n-hexane was slowly added, with partial evaporation *in vacuo*, to give a white precipitate of $[N(CH_2Ph)Et_3][PF_6]$. Filtration and further concentration gave green microcrystals. A second fractional crystallisation, from CH_2Cl_2–n-hexane, gave the pure product, yield 0.07 g (47%).

The complex $[Rh_2Cl(CO)\{P(OPh)_3\}(bipy)(\mu\text{-}RNNNR)_2][PF_6]$ was prepared similarly. Both complexes are moderately air-stable, and dissolve in CH_2Cl_2 or thf to give green solutions which slowly decompose.

Structure Determinations.—Many of the details of the structure analyses carried out on $(\mathbf{2}^+)BF_4\cdot CH_2Cl_2$ and $(\mathbf{5})\cdot 2.5CH_2Cl_2$ are listed in Table 6. *X*-Ray diffraction measurements were made on a Nicolet four-circle P3m diffractometer on single crystals mounted in thin-walled glass capillaries. Cell dimensions for each analysis were determined from the setting angle values of 15 centred reflections.

Intensity data were collected by θ—2θ scans for unique portions of reciprocal space and were corrected for Lorentz, polarisation, crystal decay (of 25 and 2%), and absorption effects. Only those reflections with pre-scan counts above a low threshold were measured for $2\theta > 40°$. The structures were solved by heavy atom (Patterson and difference Fourier) methods.

The structures were refined by blocked-cascade least squares against *F*. All non-hydrogen atoms were assigned anisotropic displacement parameters for $(\mathbf{5})\cdot 2.5CH_2Cl_2$. For $(\mathbf{2}^+)BF_4\cdot CH_2Cl_2$ all non-hydrogen atoms were assigned anisotropic displacement parameters except the tolyl and bipyridyl ring carbon atoms. Hydrogen atoms were assigned fixed isotropic displacement parameters and were constrained to ideal geometries with C–H 0.96 Å. For $(\mathbf{5})\cdot 2.5CH_2Cl_2$ the solvent molecules were severely disordered and best modelled by five chlorine sites with occupancies fixed at 0.5, together with two carbon sites also of occupancy 0.5. The resulting stoicheiometry is consistent with integration of peaks in a ^1H n.m.r. spectrum [measured for a crystalline sample of $(\mathbf{5})\cdot 2.5CH_2Cl_2$ dissolved in $CDCl_3$] for (**5**) and CH_2Cl_2. Further attempts to provide a more physically satisfactory model for the solvent molecules proved fruitless. No hydrogen atoms were included in the solvent molecules for this structure.

Final difference syntheses showed their largest features near the solvent molecules. Refinements converged smoothly to residuals given in Table 6. Tables 7 and 8 report the positional parameters. All calculations were made with programs of the SHELXTL [24] system as implemented on a Nicolet R3m/E structure determination system. Complex neutral-atom scattering factors were taken from ref. 25.

Additional material available from the Cambridge Crystallographic Data Centre, comprises H-atom co-ordinates, thermal parameters, and remaining bond lengths and angles.

Acknowledgements

We thank the S.E.R.C. for Postdoctoral Research Assistantships (to C. C. and G. G. H.) and electrochemical equipment, the Deutscher Akademischer Austauschdienst for a Scholarship (to T. B.), and Johnson Matthey for a generous loan of rhodium trichloride.

References

1 Part 29, N. G. Connelly and I. Manners, *J. Chem. Soc., Dalton Trans.*, 1989, 283.
2 N. G. Connelly, G. Garcia, M. Gilbert, and J. S. Stirling, *J. Chem. Soc., Dalton Trans.*, 1987, 1403.
3 N. G. Connelly and G. Garcia, *J. Chem. Soc., Dalton Trans.*, 1987, 2737.
4 N. G. Connelly and G. Garcia, *J. Chem. Soc., Chem. Commun.*, 1987, 246.
5 N. G. Connelly, C. J. Finn, M. J. Freeman, A. G. Orpen, and J. Stirling, *J. Chem. Soc., Chem. Commun.*, 1984, 1025.
6 T. R. Felthouse, *Prog. in Inorg. Chem.*, 1982, **29**, 73; and refs. therein.
7 N. G. Connelly, H. Daykin, and Z. Demidowicz, *J. Chem. Soc., Dalton Trans.*, 1978, 1532.
8 F. J. Lahoz, A. Tiripicchio, M. Tiripicchio-Camellini, L. A. Oro, and M. T. Pinillos, *J. Chem. Soc., Dalton Trans.*, 1985, 1487.
9 L. A. Oro, M. T. Pinillos, A. Tiripicchio, and M. Tiripicchio-Camellini, *Inorg. Chim. Acta*, 1985, **99**, L13.
10 J. L. Atwood, K. A. Beveridge, G. W. Bushnell, K. R. Dixon, D. T. Eadie, S. R. Stobart, and M. J. Zaworotko, *Inorg. Chem.*, 1984, **23**, 4050.
11 L. A. Oro, M. J. Fernandez, J. Modrego, C. Foces-Foces, and F. H. Cano, *Angew. Chem., Int. Edn. Engl.*, 1984, **23**, 913.
12 M. A. Ciriano, F. Viguri, L. A. Oro, A. Tiripicchio, and M. Tiripicchio-Camellini, *Angew. Chem., Int. Ed. Engl.*, 1987, **26**, 444.
13 D. O. K. Fjeldsted, S. R. Stobart, and M. J. Zaworotko, *J. Am. Chem. Soc.*, 1985, **107**, 8258.
14 P. K. Baker, N. G. Connelly, B. M. R. Jones, J. P. Maher, and K. R. Somers, *J. Chem. Soc., Dalton Trans.*, 1980, 579.
15 T. Brauns and A. G. Orpen, unpublished work.
16 J. L. Bear, C-L. Yao, F. J. Capdevielle, and K. M. Kadish, *Inorg. Chem.*, 1988, **27**, 3782.
17 A. C. Loyns and N. G. Connelly, unpublished work.
18 G. W. Eastland and M. C. R. Symons, *J. Chem. Soc., Dalton Trans.*, 1984, 2193.
19 J. C. Le, M. Y. Chavan, L. K. Chau, J. L. Bear, and K. M. Kadish, *J. Am. Chem. Soc.*, 1985, **107**, 7195.
20 D. C. Boyd, P. A. Matsch, M. M. Mixa, and K. R. Mann, *Inorg. Chem.*, 1986, **25**, 3331.
21 D. O. K. Fjeldsted and S. R. Stobart, *J. Chem. Soc., Chem Commun.*, 1985, 908.
22 J. C. Smart and B. L. Pinsky, *J. Am. Chem. Soc.*, 1980, **102**, 1009.
23 A. Roe, *Org. React.*, 1949, **5**, 193.
24 G. M. Sheldrick, 'SHELXTL, An Integrated System for Solving, Refining and Displaying Crystal Structures from Diffraction Data,' Revision 4.1, Nicolet Instruments Ltd, Warwick, 1983.
25 'International Tables for *X*-Ray Crystallography,' Kynoch Press, Birmingham, 1974, vol. 4.

Received 21*st September* 1988; *Paper* 8/03693D